ADVANCED QUANTUM TECHNOLOGIES
www.advquantumtech.com

Effect and Compensation of Polarization-Dependent Loss in Free-Space Reference Frame Independent Quantum Key Distribution

Kyongchun Lim, Byung-Seok Choi, Ju Hee Baek, Minchul Kim, Joong-Seon Choe, Kap-Joong Kim, Dong Churl Kim, Junsang Oh, and Chun Ju Youn**

Polarization-dependent loss (PDL) poses a critical challenge in implementing free-space quantum key distribution (QKD) systems. This study investigated the theoretical and experimental impact of PDL on polarization-encoded qubits and experimentally demonstrated a method to mitigate these effects. The proposed compensation method could effectively restore the integrity of polarization states, enhancing the robustness and security of QKD systems. Specifically, a secret key rate of 94.01% could be recovered with 5 dB PDL. This study contributes to advancing scalable and secure quantum communication technologies by addressing the critical issue of PDL in QKD systems.

1. Introduction

Quantum key distribution (QKD) represents a revolutionary advancement in secure communication, leveraging the principles of quantum mechanics to facilitate the exchange of encryption keys between two parties with theoretically unconditional security. QKD can be divided into fiber-based and free-space QKD depending on the quantum channel used for quantum state transmission.

Fiber-based QKD leverages existing optical fiber infrastructure, making it viable for urban and long-distance communications. Based on BB84, the first QKD protocol proposed by Bennett and Brassard in 1984,[1] various fiber-based QKD experiments have been reported, including laboratory[2–6] and field tests.[7–9] Significant progress has been made in extending the reach and reliability of fiber-based QKD. However, a limitation is that the secret key rate decrease exponentially with the transmission distance.[10] The twin-field QKD (TF-QKD) was proposed[11] to overcome this limitation, with reported transmission distances of 1000 km.[12]

Despite these advancements, fiber attenuation can restrict the maximum transmission distance of fiber-based QKD. In contrast, free-space QKD is particularly suitable for satellite-based communication and links where fiber deployment is impractical. It offers the advantage of potentially extending the reach of quantum communications to a global scale. Recent demonstrations of satellite-to-ground and ground-to-ground QKD have shown the potential for global quantum networking.[13,14] In addition, free-space QKD supports implementing QKD on moving platforms such as vehicles,[15] airborne,[16] and drones.[17] For moving platforms, the reference of information between the platforms can vary, degrading the QKD performance. Reference frame independent (RFI) QKD was proposed to overcome this issue.[18]

In addition, photonic chip-based QKD has emerged as a promising solution to enhance the robustness and scalability of QKD, especially in free-space environments. Photonic chips integrate QKD systems onto compact and scalable photonic platforms, offering significant advantages in terms of size, cost, and mass-production potential. Research in this domain has focused on developing integrated photonic circuits that can perform necessary quantum operations, such as state preparation, manipulation, and measurement, with high precision and stability.[19–28] These chips incorporate various components such as beam splitters, phase shifters, and single-photon detectors on a single platform, reducing the complexity and footprint of QKD systems as well as achieving the miniaturization and ruggedness required for satellite and mobile applications.

A fundamental challenge in real-world QKD system implementation is the susceptibility of quantum states, particularly polarization states, to environmental disturbances and imperfections in optical components. Polarization-dependent loss (PDL) is a perturbation that significantly affects the performance and security of QKD systems. PDL arises when optical devices exhibit differential attenuation for different polarization states, distorting the quantum states used in QKD. This phenomenon is especially problematic in practical QKD implementations, where maintaining the integrity of the polarization states is crucial for an accurate key distribution. Numerous optical compo-

K. Lim, B.-S. Choi, J. H. Baek, M. Kim, J.-S. Choe, K.-J. Kim, D. C. Kim, J. Oh, C. J. Youn
Quantum Communication Section
Electronics and Telecommunications Research Institute (ETRI)
Daejeon 34129, Republic of Korea
E-mail: lim.kc@etri.re.kr; cjyoun@etri.re.kr

The ORCID identification number(s) for the author(s) of this article can be found under https://doi.org/10.1002/qute.202400492

DOI: 10.1002/qute.202400492

nents exhibiting PDL are being used in fiber-based and free-space QKD systems. Managing and compensating for PDL becomes essential in such systems to ensure reliable and secure communication. Several related research, theoretical[29,30] and experimental,[31] have been conducted to analyze the effect of the PDL on the quantum state or QKD.

Therefore, a detailed analysis of PDL and its effects on QKD systems is required. This study delves into the theoretical and experimental aspects of polarization effect and compensation in RFI QKD, focusing on mitigating the effects of PDL. We present a simple comprehensive mathematical model to describe the effect of PDL on polarization states used in RFI QKD and propose a method to compensate for these effects. PDL compensation is commonly considered in optical communication, where it typically addresses only two polarization states such as horizontal and vertical polarization states. However, PDL compensation in RFI QKD must account for six polarization states: horizontal, vertical, diagonal, anti-diagonal, right-circular, and left-circular polarization states. To address this, we comprehensively analyze the effect of PDL and its compensation in RFI QKD by considering all six polarization states. Furthermore, while previous works on PDL effect in QKD have proposed post-selection based methods which compensate PDL effect in non-optical domain,[30,31] our method compensates for PDL in optical domain, providing fundamental compensation of PDL itself. The theoretical framework was validated through experimental setups designed to emulate PDL and test the effectiveness of the compensation technique.

By addressing the challenges posed by PDL and demonstrating viable compensation techniques, we contribute to the advancement of QKD technologies by enhancing the robustness and security of QKD systems in practical applications. Moreover, this study provides a deeper understanding of the interplay between PDL and polarization states in QKD and paves the way for more resilient implementations of QKD protocols.

2. Effect of Polarization-Dependent Loss on Polarization States in RFI QKD

To analyze the effect of PDL on the polarization encoding-based free-space RFI QKD, we first investigated how PDL can affect the polarization states generated by the transmitter of RFI QKD. We describe a mathematical model for general polarization states $|\psi\rangle$, expressed as a linear combination of the horizontal and vertical polarization states as follows:

$$|\psi\rangle = \alpha\,|H\rangle + \beta\,|V\rangle \tag{1}$$

where $|H\rangle = |0\rangle = [0,1]^T$ and $|V\rangle = |1\rangle = [1,0]^T$ represent the horizontal and vertical polarization states, respectively. α and β are selected such that $|\alpha|^2 + |\beta|^2 = 1$. Based on Equation (1), the polarization states in RFI QKD are expressed as follows[18]:

$$|H\rangle = |0\rangle$$

$$|V\rangle = |1\rangle$$

$$|D\rangle = \frac{|0\rangle + |1\rangle}{\sqrt{2}}$$

$$|A\rangle = \frac{|0\rangle - |1\rangle}{\sqrt{2}} \tag{2}$$

$$|R\rangle = \frac{|0\rangle + i\,|1\rangle}{\sqrt{2}}$$

$$|L\rangle = \frac{|0\rangle - i\,|1\rangle}{\sqrt{2}}$$

where $|H\rangle$, $|V\rangle$, $|D\rangle$, $|A\rangle$, $|R\rangle$, and $|L\rangle$ represent the horizontal, vertical, diagonal, anti-diagonal, right-circular, and left-circular polarization states, respectively. Based on Jones vector representation, we define Z basis as containing $|H\rangle$ and $|V\rangle$, X basis as containing $|D\rangle$ and $|A\rangle$, and Y basis as containing $|R\rangle$ and $|L\rangle$. As shown in Equation (2), RFI QKD utilizes a linear combination of the horizontal and vertical polarization states. These states get distorted when passing through the internal optical components of the RFI QKD because they possess a non-zero PDL. The non-zero PDL causes different losses depending on the input polarization states of the optical device. The input polarization state can be decomposed into $|H\rangle$ and $|V\rangle$ as shown in Equation (1). Here, PDL provides different losses on $|H\rangle$ and $|V\rangle$. The effect of the PDL on the polarization state can be expressed using matrix U_{PDL} as follows:[32]

$$U_{\mathrm{PDL}} = \begin{bmatrix} 1 & 0 \\ 0 & \sqrt{10^{-L_{dB}/10}} \end{bmatrix} \tag{3}$$

where L_{dB} indicates PDL in dB and can contain PDL caused by transmitter and receiver. For easy understanding, we assume the scenario where only QKD transmitter has PDL. Given the polarization state $|\psi_{\mathrm{in}}\rangle$, the polarization state $|\psi_{\mathrm{out}}\rangle$ after PDL is expressed as follows:

$$|\psi_{\mathrm{out}}\rangle = \frac{U_{\mathrm{PDL}}\,|\psi_{\mathrm{in}}\rangle}{\sqrt{\langle\psi_{\mathrm{in}}|\,U_{\mathrm{PDL}}|\psi_{\mathrm{in}}\rangle}} \tag{4}$$

This expression can be extended to a density matrix:

$$\rho_{\mathrm{out}} = \frac{U_{\mathrm{PDL}}\rho_{\mathrm{in}}U_{\mathrm{PDL}}^{\dagger}}{\mathrm{Tr}\left[U_{\mathrm{PDL}}\rho_{\mathrm{in}}U_{\mathrm{PDL}}^{\dagger}\right]} \tag{5}$$

where ρ_{out} and ρ_{in} are the density matrices of the polarization states after and before PDL, respectively.

PDL can be experimentally performed using a PDL emulator (PDLE), implemented as shown in **Figure 1**. PDLE contains two polarization beam splitters, two mirrors, and a variable optical attenuator. The first polarization beam splitter reflects and transmits the vertical and horizontal polarization states, respectively. In addition, the vertical polarization state passes through a variable optical attenuator (VOA) to attenuate its optical power. The second polarization beam splitter then combines the horizontal and vertical polarization states, forming the PDLE output. Therefore, the PDLE has the axes of PDL with horizontal and vertical polarization states, where input polarization state is decomposed into horizontal and vertical polarization components and then only vertical polarization component is attenuated by the value of PDL.

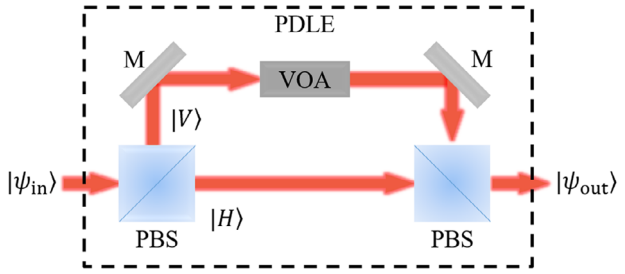

Figure 1. Structure of polarization-dependent loss (PDL) emulator. PDLE: polarization-dependent loss emulator, PBS: polarization beam splitter, VOA: variable optical attenuator.

To compensate PDL, an optical loss can be applied to the polarization states not attenuated by PDL to reduce this imbalance.[29] In other words, the same value of PDL is applied on only horizontal polarization component of the input polarization state. This can be implemented experimentally, as shown in **Figure 2**. Assume that the optical power of the vertical polarization component in the input-polarization state, given in Equation (1), is attenuated by L_{dB} using the first PDLE.

$$U_{\mathrm{PDL}}\frac{(\alpha|0\rangle+\beta|1\rangle)}{N_1}=\frac{\alpha|0\rangle+\sqrt{10^{-L_{dB}/10}}\beta|1\rangle}{N_1} \tag{6}$$

where $N_1=\sqrt{\langle\psi_{\mathrm{in}}|U_{\mathrm{PDL}}|\psi_{\mathrm{in}}\rangle}$ denotes the normalization factor. The output polarization state after the first PDLE is changed by the polarization controller U_{PC} such that

$$U_{\mathrm{PC}}\frac{\alpha|0\rangle+\sqrt{10^{-L_{dB}/10}}\beta|1\rangle}{N_1}=\frac{\alpha|1\rangle+\sqrt{10^{-L_{dB}/10}}\beta|0\rangle}{N_1} \tag{7}$$

By controlling the second PDLE such that the same PDL as that caused by the first PDLE can be applied, we can compensate PDL as follows:

$$U_{\mathrm{PDL}}\frac{\alpha|1\rangle+\sqrt{10^{-L_{dB}/10}}\beta|0\rangle}{N_1}=\sqrt{10^{-L_{dB}/10}}\frac{\alpha|1\rangle+\beta|0\rangle}{N_1} \tag{8}$$

The inversion of the horizontal and vertical polarization components can be performed using an additional polarization controller. The output optical power of the polarization state is attenuated by coefficient $\sqrt{10^{-L_{dB}/10}}$. However, using an attenuated coherent laser source does not affect the performance of QKD because the VOA is used to generate optical pulses at the single-photon level.

We implemented the experimental setup in **Figure 3** to experimentally investigate the effect and compensation of PDL on the polarization states used in RFI QKD. The setup has two parts: (1) RFI QKD transmitter and (2) PDL generator and compensator.

In the free-space RFI QKD transmitter part, six laser diodes (LDs) operate at a lasing wavelength of 1550 nm to generate the six polarization states required for RFI QKD. Electrical signals with a full width at half-maximum of 250 ps at a clock rate of 100 MHz are randomly injected into one of the six laser diodes. The output optical pulses from the laser diodes have a horizontal polarization state and are directed through polarizing beam splitters (PBS). Since PBS is designed such that the polarization state of the output port becomes horizontal (vertical) if the polarization state of the first (second) input port has a horizontal polarization state, the output polarization states of the PBS generated by LD1, LD3, and LD5 become horizontal polarization states, whereas the output polarization states of the PBS generated by LD2, LD4, and LD6 become vertical polarization states. For LD3, LD4, LD5, and LD6, an additional half-or quarter-wave plate is used to rotate the polarization. Therefore, LD1, LD2, LD3, LD4, LD5, and LD6 generate horizontal, vertical, diagonal, anti-diagonal, right-circular, and left-circular polarization states, respectively. These polarization states are collected by the two beam splitters, followed by a fixed optical attenuator. The fixed optical attenuator controls the mean photon number required for RFI QKD by lowering the optical power. However, it may block the polarization state measurements owing to its low optical power. Therefore, we did not use it in this experiment; however, it was used later in the RFI QKD experiment. The optical pulses from the laser diodes are coupled with the single-mode fiber (SMF), and then combined with the synchronization signal generated by the laser diode using a wavelength division multiplexer. The synchronization signal was not used in this experiment but will be used later in the RFI QKD experiment.

In the PDL generator and compensator part, the output optical pulses from the free-space RFI QKD transmitter are transmitted to the polarization controller, followed by the first PDLE. The polarization controller in the PDL generator compensates for the polarization state change generated by the free-space RFI QKD transmitter by the SMF[33] such that the input polarization state of the first PDLE becomes a horizontal, vertical, diagonal, anti-diagonal, right-circular, or left-circular polarization state. The first PDLE then applies the PDL to the input polarization state. The polarization controller in the PDL compensator changes the horizontal and vertical components of the input polarization state, as shown in Equation (7) and PDLE applies the same PDL as that applied by the first PDLE, as in Equation (8). Finally, three wave-

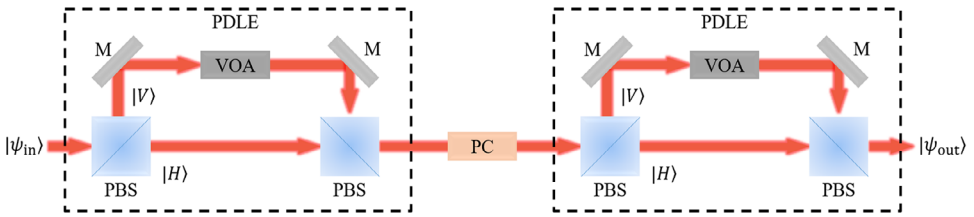

Figure 2. PDL compensation process. PDLE: polarization-dependent loss emulator, PBS: polarization beam splitter, VOA: variable optical attenuator, PC: polarization controller.

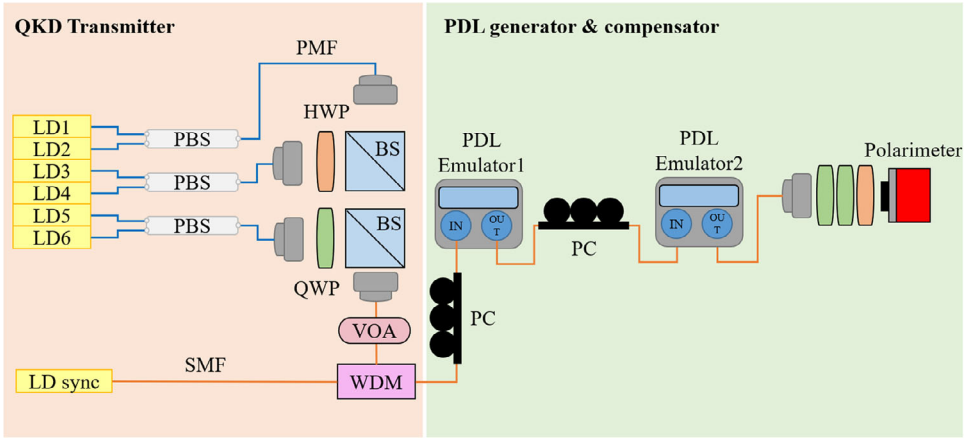

Figure 3. Experimental setup for PDL effect and compensation for polarization states in reference frame independent (RFI) quantum key distribution (QKD). LD: laser diode, PBS: polarization beam splitter, PMF: polarization maintaining fiber, BS: 50:50 beam splitter, HWP: half-wave plate, QWP: quarter-wave plate, VOA: variable optical attenuator, SMF: single-mode fiber, WDM: wavelength division multiplexer, PC: polarization controller.

plates are placed to compensate for the polarization rotation by SMF, and the output polarization state is then measured by the polarimeter, providing the Stokes parameters.

Once PDL of L_{dB} is applied by the first PDLE on a input polarization state of the first PDLE, output polarization state of the first PDLE can be changed and we denote its density matrix by $\rho_1(L_{\mathrm{dB}})$. Then, $\rho_1(L_{\mathrm{dB}})$ is measured by the polarimeter providing the corresponding Stokes parameters, $s_1(L_{\mathrm{dB}})$, $s_2(L_{\mathrm{dB}})$, and $s_3(L_{\mathrm{dB}})$. Based on these Stokes parameters, we can construct $\rho_1(L_{\mathrm{dB}})$.[34]

$$\rho_1(L_{\mathrm{dB}}) = \frac{1}{2}\left[I_2 + s_1(L_{\mathrm{dB}})\sigma_X + s_2(L_{\mathrm{dB}})\sigma_Y + s_3(L_{\mathrm{dB}})\sigma_Z\right] \tag{9}$$

where I_2 is a 2×2 identity matrix and σ_X, σ_Y, and σ_Z are the Pauli matrices. Similarly, the polarization state after compensation by the second PDLE, $\rho_2(L_{\mathrm{dB}})$ can be obtained using the measured Stokes parameters.

To investigate the extent to which a polarization state can be distorted and compensated, we calculated the fidelity for two cases: 1) $F(\rho_1(0), \rho_1(L_{\mathrm{dB}}))$ and 2) $F(\rho_1(0), \rho_2(L_{\mathrm{dB}}))$. Here, fidelity $F(\rho_X, \rho_Y)$ is calculated as follows:

$$F(\rho_X, \rho_Y) = \left(\mathrm{Tr}\sqrt{\sqrt{\rho_X}\rho_Y\sqrt{\rho_X}}\right)^2 \tag{10}$$

$F(\rho_X, \rho_Y) = \mathrm{Tr}(\rho_X\rho_Y)$ if ρ_X or ρ_Y is a pure state. Since the degree of polarization of the laser diode used in this experiment is almost 100%, we assumed $\rho_1(0)$ to be a pure state and applied the fidelity expression mentioned above.

The corresponding results are shown in **Figure 4**. Each subfigure shows the fidelity with and without compensation, depending on the applied PDL with respect to the polarization state generated by the free-space RFI QKD transmitter. During this experiment, each polarization state is individually generated.

Note that vertical scale of Figure 4a,b is from 0.99 to 1.01, while vertical scale of Figure 4c–f is from 0.75 to 1.05. Since the output polarization state of the PDLE remains unchanged when the input polarization state of the PDLE is either horizontal or vertical, the results show that the both horizontal and vertical polarization states are almost unaffected by the PDLE. However, the fidelity of the vertical polarization state is slightly reduced after 6 dB PDL. Since the vertical polarization state generated by the free-space RFI QKD transmitter is not ideal, meaning that a small horizontal component of the polarization state exists, the horizontal component of the input polarization state appears to increase as the applied PDL increases, lowering the fidelity. For linear combinations of horizontal and vertical polarization states, namely diagonal, anti-diagonal, right-circular, and left-circular polarization states, the fidelity decreases as the applied PDL increases. At 10 dB PDL, their fidelities are lowered by approximately 20% from that without PDL. This may significantly compromise the security of a QKD system by destroying mutual unbiasedness among the polarization states generated by the QKD system and increasing the quantum bit error rate (QBER).

In addition, we confirmed that the lowered fidelity can be compensated so that the fidelity is almost recovered, even with the PDL applied. Therefore, we expect that the security and performance of a QKD system can be maintained under PDL.

3. Effect of Polarization-Dependent Loss on RFI QKD

3.1. Decoy-State RFI QKD

This section introduces the decoy-state RFI QKD. In the decoy-state RFI QKD using polarization encoding, a transmitter Alice prepares one of the polarization states in Equation (2) and transmits it to a receiver Bob. In the decoy method the probability of preparation can be decomposed into three parts: basis, state, and signal intensity. For $a \in \{Z, X, Y\}$, $x \in \{0, 1\}$, and $i \in \{\mu, \nu, w\}$, the probabilities that Alice chooses basis, state, and signal intensity can be expressed as P_a^A, P_x, and P_i, respectively. Similarly, for $b \in \{Z, X, Y\}$ and $y \in \{0, 1\}$, the probabilities that Bob chooses basis and measures state can be expressed as P_b^B and P_y, respectively. In general, the state is chosen to maximize the entropy, i.e., $P_x = 1/2$. The prepared polarization state with basis a and state x is measured by Bob through free space and receiver, which are modeled as quantum channels with transmittance $\eta_{a_x b_Y}$ for

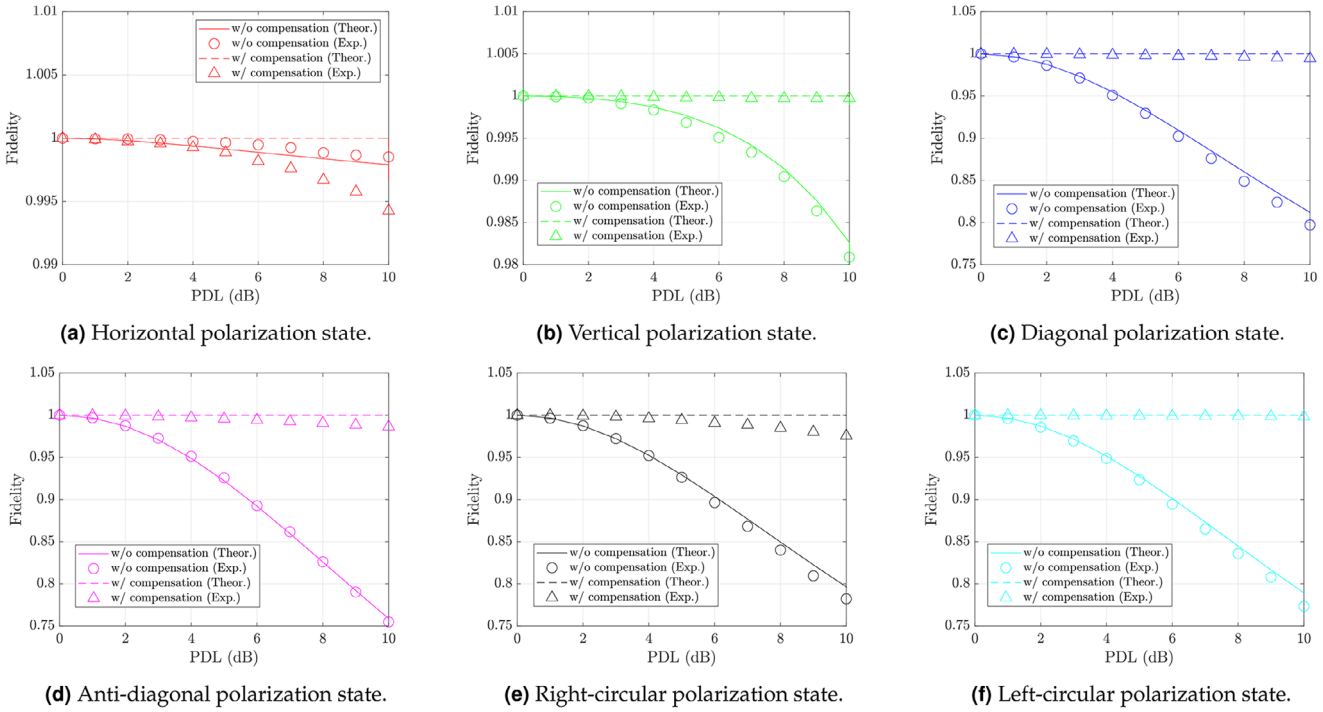

(a) Horizontal polarization state. **(b)** Vertical polarization state. **(c)** Diagonal polarization state.

(d) Anti-diagonal polarization state. **(e)** Right-circular polarization state. **(f)** Left-circular polarization state.

Figure 4. Fidelity with respect to the applied PDL by the first PDLE depending on the polarization state generated by the free-space RFI QKD.

$a, b \in \{Z, X, Y\}$ and $x, y \in \{0, 1\}$.

$$\eta_{a_x b_Y} = 10^{\frac{-L_{FS}}{10}} 10^{\frac{-L_{Rx}}{10}} \eta_D T_{a_x b_y} \tag{11}$$

where L_{FS}, L_{RX}, and η_D represent the optical loss of free space, internal optical loss of the receiver in dB, and detection efficiency of a single-photon detector, respectively. Considering that the probability of choosing Bob's basis is P_b^B, $T_{a_x b_y}$ indicates the theoretical probability that, when Alice prepares the polarization state with basis a and state x, Bob measures it with basis b and obtains state y.[35] Specifically, this can be expressed depending on the relation between a and b. For the case where bases of Alice and Bob are the same, $a = b$,

$$T_{a_x b_y} = \begin{cases} 1 - e_{\text{det}} & \text{for } x = y \\ e_{\text{det}} & \text{for } x \neq y \end{cases} \tag{12}$$

For the case where bases of Alice and Bob are different, $a \neq b$,

$$T_{a_x b_y} = \begin{cases} \frac{1}{2} & \text{for } x = y \\ \frac{1}{2} & \text{for } x \neq y \end{cases} \tag{13}$$

where e_{det} indicates the intrinsic QBER which can be experimentally obtained when a quantum channel between Alice and Bob has a loss of 0 dB.

Suppose that Alice uses a weak coherent laser source whose photon number statistics follow Poisson distribution in decoy-state RFI QKD. Alice prepares the polarization state with basis a, state s, and signal intensity i and Bob measures it with basis b and obtains state y. Then, the overall counting probability $Q^i_{a_x b_y}$ is given by

$$Q^i_{a_x b_y} = 1 - (1 - Y_0) e^{-i\eta_{a_x b_y}} \tag{14}$$

where Y_0 represents the dark count probability of the single-photon detector. Accordingly, when Alice and Bob choose bases a and b, respectively, for signal intensity i, the overall counting probability Q^i_{ab} and erroneous counting probability W^i_{ab} can be expressed as follows:

$$Q^i_{ab} = \frac{1}{2}\left(Q^i_{a_0 b_0} + Q^i_{a_0 b_1} + Q^i_{a_1 b_0} + Q^i_{a_1 b_1}\right) \tag{15}$$

$$W^i_{ab} = \frac{1}{2}\left(Q^i_{a_0 b_1} + Q^i_{a_1 b_0}\right) \tag{16}$$

When Alice and Bob choose a and b bases, respectively, for signal intensity i, QBER E^i_{ab} is given by W^i_{ab}/Q^i_{ab}. To apply the decoy-state method,[35–37] we defined the lower bound of the single- and zero-photon counting probabilities and the upper bound of QBER caused by a single photon. $s_{ab,0}$ and $s_{ab,1}$ represent the lower bound of a single-photon and zero-photon counting probability, respectively, given that Alice transmits a zero- or a single-photon state and can be expressed as follows:

$$s_{ab,0} = \max\left[\frac{\nu e^w Q^w_{ab} - w e^\nu Q^\nu_{ab}}{\nu - w}, 0\right] \tag{17}$$

$$s_{ab,1} = \max\left[\frac{\mu}{\mu(\nu - w)) - \nu^2 + w^2}\left\{e^\nu Q^\nu_{ab} - e^w Q^w_{ab} - \frac{\nu^2 - w^2}{\mu^2}\left(e^\mu Q^\mu_{ab} - s_{ab,0}\right)\right\}, 0\right] \tag{18}$$

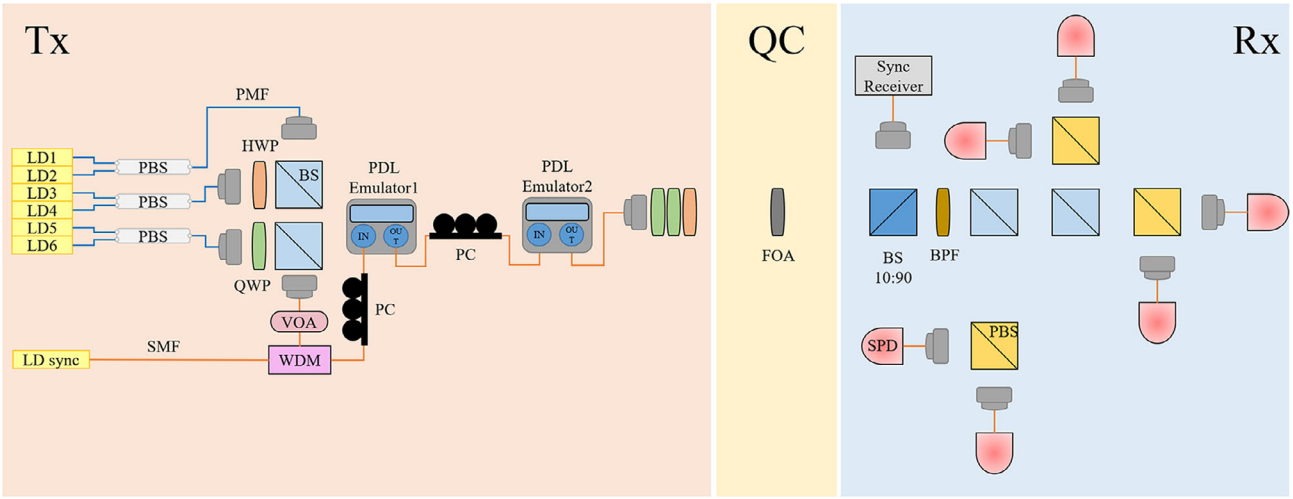

Figure 5. Experimental setup to analyze PDL effect and compensate for RFI QKD. LD: laser diode, PBS: polarization beam splitter, PMF: polarization maintaining fiber, BS: 50:50 beam splitter, HWP: half-wave plate, QWP: quarter-wave plate, VOA: variable optical attenuator, SMF: single-mode fiber, WDM: wavelength division multiplexer, PC: polarization controller, QC: quantum channel, FOA: fixed optical attenuator, BPF: bandpass filter, SPD: single photon detector.

The upper bound of QBER caused by a single photon, e_{ab}, is given by

$$e_{ab} = \min\left[\frac{e^{v}W^{v}_{ab} - e^{w}W^{w}_{ab}}{(v-w)s_{ik,1}}, \frac{1}{2}\right] \tag{19}$$

To estimate information leakage to an eavesdropper, Eve, RFI QKD utilizes the security parameter C.

$$C = \left(1-2e_{ZZ}\right)^2 + \left(1-2e_{ZX}\right)^2 + \left(1-2e_{XZ}\right)^2 + \left(1-2e_{XX}\right)^2 \tag{20}$$

C is independent of the rotation angle of the reference of polarization.[18] Based on C, Alice and Bob can estimate the information leakage due to eavesdropping I_E as follows:

$$I_E = (1-e_{YY})H\left(\frac{1+u}{2}\right) + e_{YY}H\left(\frac{1+v}{2}\right) \tag{21}$$

where

$$u = \min\left[\frac{1}{1-e_{Y_AY_B}}\sqrt{\frac{C}{2}}, 1\right] \tag{22}$$

$$v = \frac{1}{e_{Y_AY_B}}\sqrt{\frac{C}{2} - (1-e_{Y_AY_B})^2u^2} \tag{23}$$

and $H(\cdot)$ represents the binary entropy.

Then, the secret key rate for the decoy-state RFI QKD R in the asymptotic regime[35,37] can be calculated as follows:

$$R = P_\mu P^A_Y P^B_Y\left[-fQ^\mu_{YY}H(E^\mu_{YY}) + \mu e^\mu s_{YY,1}(1-I_E)\right] \tag{24}$$

3.2. Experimental Setup

For the experiment of RFI QKD under PDL, we implemented the setup in **Figure 5**. The transmitter used is the same as that shown in Figure 3 with VOA to control the mean photon number of the quantum signal and a synchronization signal to synchronize the transmitter and receiver signals. The signal leaving the free-space RFI QKD transmitter is transmitted through a quantum channel modeled as a variable optical attenuator to emulate the optical channel loss of the free-space channel. At the free-space RFI QKD receiver, the incoming signal initially encounters a 10:90 beam splitter, which divides it into quantum and synchronization signals. The reflected portion is utilized for clock synchronization between the transmitter and receiver. The transmitted portion is passed through an optical bandpass filter with a full width at half maximum of 2 nm to separate the synchronization and quantum signals. The filtered quantum signals were subsequently processed using decoding components, including a beam splitter, PBS, and wave plates. Finally, the decoded signal is directed to an InGaAs avalanche photodiode-based single-photon detector through SMF. All controls and data processing in this experiment were managed using an FPGA for real-time measurements of QBERs and sifted key rates.

Table 1. Parameters for calculating the secret key rate R.

P_μ	P_ν	P_w	P^A_Y	P^A_X	P^A_Z	P^B_Y	P^B_X	P^B_Z	L_{Rx}	e_{det}	η_D	f	ν	w	P_{dark}
1/3	1/3	1/3	1/3	1/3	1/3	1/2	1/4	1/4	7.58	0.01	0.076	1.16	0.1	0	2×10^{-6}

The experimental parameters were chosen or measured, as shown in **Table 1**. Based on these parameters, signal intensity μ is optimized to maximize the secret key rate.

3.3. Experimental Results

The previous results show PDL can distort the polarization state generated by the free-space RFI QKD transmitter and can be compensated, but it cannot directly measure the effect of PDL on the RFI QKD performance. Therefore, we performed a free-space RFI QKD experiment to verify the effect of PDL on the RFI QKD performance.

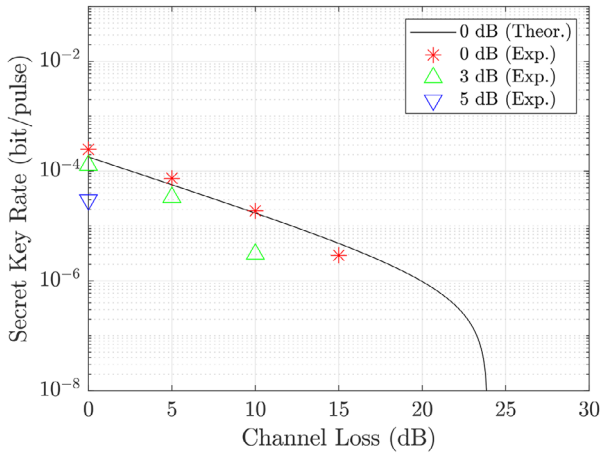

(a) Without PDL compensation.

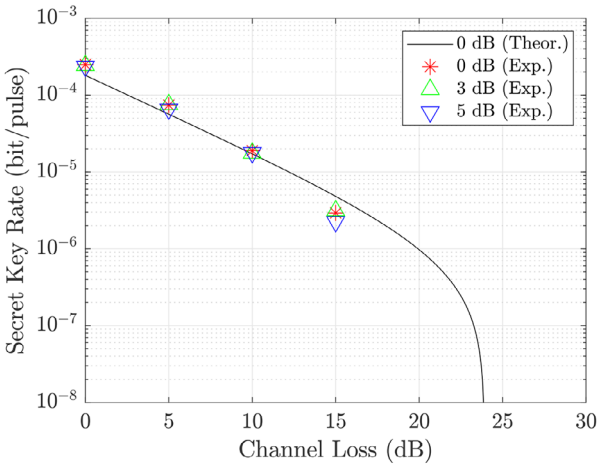

(b) With PDL compensation.

Figure 6. Secret key rate with respect to the optical channel loss depending on the applied PDL.

Figure 6 shows the secret key rate with respect to the optical channel loss between Alice and Bob depending on PDL compensation. In Figure 6a, experimental results under 0 dB PDL well match the theoretical results. However, depending on the applied non-zero PDL, its secret key rate significantly deviates from that under 0 dB PDL. In particular, under 5 dB PDL, we find that a secret key rate cannot be generated with more than 3 dB channel loss. However, this degradation of the secret key rate by PDL can be restored by PDL compensation, as shown in Figure 6b. Specifically, by compensating for the PDL, we experimentally identified that a secret key rate with 5 dB applied PDL at 10 dB channel loss can be dramatically recovered to 94.01% of the secret key rate without PDL. The experimental results indicate that a small PDL can significantly degrade the secret key rate but can be recovered by PDL compensation.

4. Conclusion

This study demonstrated the significant effect of PDL on the security and performance of free-space QKD systems. Through comprehensive analysis and experimental validation, we highlight the challenges PDL poses in distorting the polarization states, which are crucial for reliable QKD. This can be experimentally verified using RFI QKD. Specifically, when 5 dB PDL is applied, RFI QKD, which is capable of generating secret keys with over 15 dB channel loss, fails to generate any secret keys once channel loss exceed 3 dB. Through this experimental observation, we confirm that PDL can significantly limit the performance of RFI QKD, highlighting the necessity for PDL compensation method. We also experimentally proved that the PDL compensation effectively mitigates these distortions, ensuring the robustness and security of QKD in practical implementations. The result of this work can be applied in real-world scenario as follows: First, PDL of a QKD transmitter is characterized using the method described in ref. [31], providing a quantified PDL value. Subsequently, PDL compensation can be achieved by applying an equal amount of PDL to counterbalance. This work provides a deeper understanding of PDL's effects on quantum states and offers viable solutions for enhancing the reliability of free-space QKD systems, paving the way for more resilient and scalable quantum communication networks.

Acknowledgements

This work was supported by the Institute of Information & communications Technology Planning & Evaluation(IITP) grant funded by the Korea government(MSIT) (RS-2019-II190005, Technology development of transmitter and receiver integrated module in a polarization based free-space quantum key distribution for short-range low-speed moving quantum communication), (RS-2020-II200890, Development of trusted node core and interfaces for the interoperability among QKD protocols), (RS-2022-II221014, Technology development of lightweight free space quantum repeating platform), (RS-2024-00398716, Development of 30km Longrange Free-space Quantum Key Distribution System and Core-technologies for Satellite Quantum Secure Communication).

Conflict of Interest

The authors declare no conflict of interest.

Data Availability Statement

The data that support the findings of this study are available from the corresponding author upon reasonable request.

Keywords

polarization dependent loss, quantum key distribution, reference frame independent quantum key distribution

Received: September 29, 2024
Revised: November 22, 2024
Published online: December 31, 2024

[1] C. H. Bennett, G. Brassard, *Theo. Comput. Sci.* **2014**, *560*, 7.
[2] P. A. Hiskett, D. Rosenberg, C. G. Peterson, R. J. Hughes, S. Nam, A. E. Lita, A. J. Miller, J. E. Nordholt, *New J. Phys.* **2006**, *8*, 193.

[3] L. C. Comandar, B. Fröhlich, M. Lucamarini, K. A. Patel, A. W. Sharpe, J. F. Dynes, Z. L. Yuan, R. V. Penty, A. J. Shields, *Appl. Phys. Lett.* **2014**, *104*, 021101.
[4] B. Fröhlich, M. Lucamarini, J. F. Dynes, L. C. Comandar, W. W.-S. Tam, A. Plews, A. W. Sharpe, Z. Yuan, A. J. Shields, *Optica* **2017**, *4*, 163.
[5] H.-L. Yin, P. Liu, W.-W. Dai, Z.-H. Ci, J. Gu, T. Gao, Q.-W. Wang, Z.-Y. Shen, *Opt. Express* **2020**, *28*, 29479.
[6] Y. Chen, C. Huang, Z. Chen, W. He, C. Zhang, S. Sun, K. Wei, *Phys. Rev. A* **2022**, *106*, 022614.
[7] A. R. Dixon, J. F. Dynes, M. Lucamarini, B. Fröhlich, A. W. Sharpe, A. Plews, W. Tam, Z. L. Yuan, Y. Tanizawa, H. Sato, S. Kawamura, M. Fujiwara, M. Sasaki, A. J. Shields, *Sci. Rep.* **2017**, *7*, 1978.
[8] D. Bacco, I. Vagniluca, B. D. Lio, N. Biagi, A. D. Frera, D. Calonico, C. Toninelli, F. S. Cataliotti, M. Bellini, L. K. Oxenløwe, A. Zavatta, *EPJ Quantum Technol.* **2019**, *6*, 5.
[9] M. Avesani, L. Calderaro, G. Foletto, C. Agnesi, F. Picciariello, F. B. L. Santagiustina, A. Scriminich, A. Stanco, F. Vedovato, M. Zahidy, G. Vallone, P. Villoresi, *Opt. Lett.* **2021**, *46*, 2848.
[10] S. Pirandola, R. Laurenza, C. Ottaviani, L. Banchi, *Nat. Commun.* **2017**, *8*, 15043.
[11] M. Lucamarini, Z. L. Yuan, J. F. Dynes, A. J. Shields, *Nature* **2018**, *557*, 400.
[12] Y. Liu, W.-J. Zhang, C. Jiang, J.-P. Chen, C. Zhang, W.-X. Pan, D. Ma, H. Dong, J.-M. Xiong, C.-J. Zhang, H. Li, R.-C. Wang, J. Wu, T.-Y. Chen, L. You, X.-B. Wang, Q. Zhang, J.-W. Pan, *Phys. Rev. Lett.* **2023**, *130*, 210801.
[13] S.-K. Liao, W.-Q. Cai, W.-Y. Liu, L. Zhang, Y. Li, J.-G. Ren, J. Yin, Q. Shen, Y. Cao, Z.-P. Li, F.-Z. Li, X.-W. Chen, L.-H. Sun, J.-J. Jia, J.-C. Wu, X.-J. Jiang, J.-F. Wang, Y.-M. Huang, Q. Wang, Y.-L. Zhou, L. Deng, T. Xi, L. Ma, T. Hu, Q. Zhang, Y.-A. Chen, N.-L. Liu, X.-B. Wang, Z.-C. Zhu, C.-Y. Lu, et al., *Nature* **2017**, *549*, 43.
[14] Y.-A. Chen, Q. Zhang, T.-Y. Chen, W.-Q. Cai, S.-K. Liao, J. Zhang, K. Chen, J. Yin, J.-G. Ren, Z. Chen, S.-L. Han, Q. Yu, K. Liang, F. Zhou, X. Yuan, M.-S. Zhao, T.-Y. Wang, X. Jiang, L. Zhang, W.-Y. Liu, Y. Li, Q. Shen, Y. Cao, C.-Y. Lu, R. Shu, J.-Y. Wang, L. Li, N.-L. Liu, F. Xu, X.-B. Wang, et al., *Nature* **2021**, *589*, 214.
[15] J.-P. Bourgoin, B. L. Higgins, N. Gigov, C. Holloway, C. J. Pugh, S. Kaiser, M. Cranmer, T. Jennewein, *Opt. Express* **2015**, *23*, 33437.
[16] C. J. Pugh, S. Kaiser, J.-P. Bourgoin, J. Jin, N. Sultana, S. Agne, E. Anisimova, V. Makarov, E. Choi, B. L. Higgins, T. Jennewein, *Quant. Sci. Technol.* **2017**, *2*, 024009.
[17] A. Conrad, S. Isaac, R. Cochran, D. Sanchez-Rosales, T. Rezaei, T. Javid, A. J. Schroeder, G. Golba, D. Gauthier, P. Kwiat, in *Quantum Computing, Communication, and Simulation III*, (Eds.: P. R. Hemmer, A. L. Migdall), vol. *12446*, International Society for Optics and Photonics, SPIE, **2023**, p. 124460H.
[18] A. Laing, V. Scarani, J. G. Rarity, J. L. O'Brien, *Phys. Rev. A* **2010**, *82*, 012304.
[19] P. Sibson, C. Erven, M. Godfrey, S. Miki, T. Yamashita, M. Fujiwara, M. Sasaki, H. Terai, M. G. Tanner, C. M. Natarajan, R. H. Hadfield, J. L. O'Brien, M. G. Thompson, *Nat. Commun.* **2017**, *8*, 13984.
[20] F. Beutel, H. Gehring, M. A. Wolff, C. Schuck, W. Pernice, *npj Quantum Inf.* **2021**, *7*, 40.
[21] T. K. Paraïso, T. Roger, D. G. Marangon, I. D. Marco, M. Sanzaro, R. I. Woodward, J. F. Dynes, Z. Yuan, A. J. Shields, *Nat. Photon.* **2021**, *15*, 850.
[22] G. Vest, P. Freiwang, J. Luhn, T. Vogl, M. Rau, L. Knips, W. Rosenfeld, H. Weinfurter, *Phys. Rev. Appl.* **2022**, *18*, 024067.
[23] R. Sax, A. Boaron, G. Boso, S. Atzeni, A. Crespi, F. Grünenfelder, D. Rusca, A. Al-Saadi, D. Bronzi, S. Kupijai, H. Rhee, R. Osellame, H. Zbinden, *Photon. Res.* **2023**, *11*, 1007.
[24] C.-X. Zhu, Z.-Y. Chen, Y. Li, X.-Z. Wang, C.-Z. Wang, Y.-L. Zhu, F.-T. Liang, W.-Q. Cai, G. Jin, S.-K. Liao, C.-Z. Peng, *Phys. Rev. Appl.* **2022**, *17*, 064034.
[25] Y. Du, X. Zhu, X. Hua, Z. Zhao, X. Hu, Y. Qian, X. Xiao, K. Wei, *Chip* **2023**, *2*, 100039.
[26] K. Wei, X. Hu, Y. Du, X. Hua, Z. Zhao, Y. Chen, C. Huang, X. Xiao, *Photon. Res.* **2023**, *11*, 1364.
[27] Y. Du, B.-H. Li, X. Hua, X.-Y. Cao, Z. Zhao, F. Xie, Z. Zhang, H.-L. Yin, X. Xiao, K. Wei, *arXiv preprint arXiv:2407.07513* **2024**.
[28] K. Lim, B.-S. Choi, J.-S. Choe, J. H. Baek, M. Kim, K.-J. Kim, C. J. Youn, *Optical Fiber Communication Conference (OFC)*, **2023**.
[29] R. A. Brewster, B. T. Kirby, J. D. Franson, M. Brodsky, *Phys. Rev. A* **2019**, *100*, 033811.
[30] C. Li, M. Curty, F. Xu, O. Bedroya, H.-K. Lo, *Phys. Rev. A* **2018**, *98*, 042324.
[31] C. Huang, Y. Chen, L. Jin, M. Geng, J. Wang, Z. Zhang, K. Wei, *Phys. Rev. A* **2022**, *105*, 012421.
[32] N. Cui, X. Zhang, W. Zhang, X. Tang, L. Xi, *Appl. Sci.* **2020**, *10*, 3844.
[33] F. Treviño-Martínez, D. Tentori, C. Ayala-Díaz, F. J. Mendieta-Jiménez, *Opt. Express* **2005**, *13*, 2556.
[34] R. T. Thew, K. Nemoto, A. G. White, W. J. Munro, *Phys. Rev. A* **2002**, *66*, 012303.
[35] H. Liu, J. Wang, H. Ma, S. Sun, *Phys. Rev. Appl.* **2019**, *12*, 034039.
[36] X. Ma, B. Qi, Y. Zhao, H.-K. Lo, *Phys. Rev. A* **2005**, *72*, 012326.
[37] J. Zhu, C. Zhang, Q. Wang, *Eur. Phys. J. D* **2017**, *71*, 319.